Korean J. Chem. Eng., **21**(4), 782-792 (2004)

A Hybrid Adsorbent-Membrane Reactor (HAMR) System for Hydrogen Production

Byoung-Gi Park†

Department of Chemical Engineering, University of Southern California, HED216, Los Angeles, CA90089-1211, California, USA
(*Received 9 February 2004 • accepted 28 April 2004*)

Abstract−Design characteristics and performance of a novel reactor system, termed a hybrid adsorbent-membrane reactor (HAMR), have been investigated for hydrogen production. The recently proposed HAMR concept couples reactions and membrane separation steps with adsorption on the membrane feed-side or permeate-side. Performance of conventional reactors has been significantly improved by this integrated system. In this paper, an HAMR system has been studied involving a hybrid-type packed-bed catalytic membrane reactor undergoing methane steam reforming through a porous ceramic membrane with a CO_2 adsorption system. This HAMR system is of potential interest to pure hydrogen production for fuel cells for various mobile and stationary applications. Reactor behaviors have been investigated for a range of temperature and pressure conditions. The HAMR system shows enhanced methane conversion, hydrogen yield, and product purity, and provides good promise for reducing the hostile operating conditions of conventional reformers, and for meeting the product purity requirements.

Key words: Membrane, Membrane Reactor, Methane-Steam Reforming, Hydrogen Production, Equilibrium-Shift

INTRODUCTION

As a result of enhanced environmental regulations worldwide, hydrogen is progressively becoming a very important clean energy source for both mobile and stationary applications. For hydrogen to replace fossil fuels as the fuel of choice for mobile applications, it will require the creation of a production and delivery infrastructure for hydrogen equivalent to those that currently exist for fossil fuels and natural gas. As an alternative, and as an interim step leading towards the new hydrogen economy, various groups are currently investigating hydrocarbon steam reforming for on-board generation of hydrogen to use in fuel-cell-powered vehicles, or for on-site production in stead of incompressible hydrogen gas storage for power generation applications [Choi and Stenger, 2003; Darwish et al., 2003; Liu et al., 2002; Semelsberger et al., 2003].

Methane-steam reforming is currently attracting renewed interest in this regard, particularly for distributed power generation through the use of fuel cells. The process is widely practiced for large-scale hydrogen production, and involves reacting steam with methane, through the endothermic and reversible methane steam reforming, over supported nickel catalysts in packed-bed reactors. Traditionally, these reformers have been generally operated at very severe conditions, utilizing temperatures often in excess of 1,000 K, pressures as high as 30 bar, and reach relatively low equilibrium conversions [Elnashaie et al., 1990; Froment and Bischoff, 1990; Nam et al., 2000; Xu and Froment, 1989].

These conditions are often not convenient or economic to attain for small-scale, on-site or on-board hydrogen generation. As a result, there are current attempts to develop more effective reforming technologies. Reactive separation processes have been proposed as alternative ways of catalytic steam reforming. Their potential advantages have been widely discussed over the conventional reactors. These include membrane reactors [Hwang, 2001; Nam et al., 2000; Saracco and Specchia, 1994; Sanchez and Tsotsis, 2002], more recently adsorptive reactors [Ding and Alpay, 2000a, b; Han and Harrison, 1994; Lee et al., 2004; Xiu et al., 2002, 2003], or even fluidized bed adsorptive membrane reactors [Prasad and Elnashaie, 2004]. They include (i) increasing reactant conversion and product yield, through shifting the equilibrium towards the products. This, potentially, allows one to operate under milder operating conditions (e.g., lower temperature and pressures, and reduced level of catalyst coking); (ii) reducing the downstream purification requirements by *in situ* separation of the desired product hydrogen, in the case of membrane reactors, or the undesired product CO_2, in the case of adsorptive reactors, from the reaction mixture.

Membrane reactors show substantial promise in this area and typically utilize nano-porous inorganic or metallic Pd or Pd-alloy membranes [Hwang, 2001; Nam et al., 2000]. The latter are better suited for pure hydrogen production. However, metallic membranes are very expensive and become brittle during reactor operation, or deactivated in the presence of sulfur or coke. Even though the nano-porous membranes are better suited for the steam reforming environment, they are, however, difficult to manufacture without cracks and pin-holes, and as a result often show inferior product yield. In addition, the hydrogen product in the permeate-side contains substantial amounts of other byproducts, particularly CO_2, and may require further treatment for use in fuel-cell-powered vehicles.

Adsorptive methane steam reforming reactors also show good potential [Ding and Alpay, 2000a, b; Han and Harrison, 1994; Lee et al., 2004; Prasad and Elnashaie, 2004; Xiu et al., 2002, 2003]. The challenge here is in matching the adsorbent properties with those of the catalytic system. For high temperature CO_2 removals, typically two types of adsorbents, e.g. CaO and potassium promoted layered-double hydrotalcite, have been suggested [Ding and Alpay, 2000a, b; Han and Harrison, 1994; Lee et al., 2004; Prasad and El-

†To whom correspondence should be addressed.
E-mail: byounggi@petro.lg.co.kr

nashaie, 2004; Xiu et al., 2002, 2003]. CaO utilizing its carbonation reaction, can be used at the typical steam reforming temperatures, but requires temperature over 1,000 K for regeneration [Knacke et al., 1991]. This is a very harsh regeneration condition, which may result in gradual deterioration of the adsorbent properties and potential sintering of the reforming catalyst. The mismatch between the reaction and regeneration conditions is likely to result, furthermore, in significant process complications. More recently, a potassium promoted layered-double hydrotalcite has been proposed as an alternative to the aforementioned CaO adsorbent, which is also appropriate for high temperature CO_2 adsorption [Ding and Alpay, 2000a, b; Xiu et al., 2002, 2003]. An advantage of the potassium promoted hydrotalcite adsorbent is the range of regeneration temperature as low as from 473 K to 723 K [Ding and Alpay, 2000a, b].

Here what we propose for use, instead, is a novel new reactor system, termed the hybrid adsorbent-membrane reactor (HAMR) system. The HAMR concept, which was recently proposed by our group [Park and Tsotsis, 2004], couples the reaction and membrane separation steps with adsorption on the reactor and/or membrane permeate-side. The previously investigated HAMR system involves a hybrid pervaporation membrane reactor system integrating reversible esterification and pervaporation steps through a membrane with water adsorption. Coupling reaction, pervaporation and adsorption significantly improved performance of conventional membrane reactors, and reduced temperature conditions.

In this paper we are proposing a novel conceptual HAMR system involving a hybrid-type packed-bed catalytic membrane reactor coupling the methane steam reforming reaction through a porous ceramic membrane with a high temperature CO_2 adsorption system suitable for low temperature regeneration. This HAMR system shows behavior that is more advantageous than either the membrane reactors or the adsorptive reactors in terms of the attained yield and selectivity. In addition, the HAMR system potentially allows significantly greater process flexibility than either the membrane or the adsorptive reactor system. Compared to the adsorptive reactors, the membrane, for example, can be used as a barrier to separate the catalyst from the adsorbent phases, thus allowing for *in situ* continuous regeneration of the adsorbent. Moreover, it can be expected to reduce cost of hydrogen purification by means of enrichment of product hydrogen in one side of the HAMR utilizing *in situ* membrane separation. The HAMR system shows, furthermore, significant potential advantages with respect to the conventional membrane reactor (MR) system. Beyond the improved yield and selectivity, the HAMR system has the potential for producing a CO_2-free fuel-cell grade hydrogen product in lower temperature conditions compared to the conditions for other types of reformers, which is of significance for the proposed fuel-cell based mobile or stationary applications of such systems.

In this preliminary research, a mathematical model for the HAMR system is presented and analyzed, for a range of temperature and pressure conditions. The behavior of the HAMR system is compared with the conventional packed-bed reactor, as well as a conventional membrane reactor.

THEORY

1. Kinetics for Methane-Steam Reforming

For methane steam reforming, we have utilized a catalytic reaction scheme proposed by Xu and Froment [Froment and Bischoff, 1990; Xu and Froment, 1989], which has since found wide-spread application. According to Xu and Froment [Froment and Bischoff, 1990; Xu and Froment, 1989] (see also Elnashaie et al., 1990; Nam et al., 2000), the methane-steam reforming consists of two major endothermic reforming reaction steps, together with an exothermic water-gas shift reaction (see Table 1). The overall reaction is highly endothermic. The rate expressions, heats of reactions, and the thermodynamic parameters for the three reaction steps are shown in Table 1. The kinetic parameters, as reported by Xu and Froment [Froment and Bischoff, 1990; Xu and Froment, 1989], are summarized in Table 2. Formation rates for the H_2, CO and CO_2 products and disappearance rates for CH_4 and water are given by the following equations:

$$r_{H_2} = +3r_1 + r_2 + 4r_3 \quad (1)$$

$$r_{CO} = +r_1 - r_2 \quad (2)$$

$$r_{CO_2} = +r_2 + r_3 \quad (3)$$

$$r_{CH_4} = -r_1 - r_3 \quad (4)$$

$$r_{H_2O} = -r_1 - r_2 - 2r_3 \quad (5)$$

2. The Mathematical Model of the HAMR System

A schematic of an experimental setting for the HAMR system

Table 1. Rate expressions and thermodynamic properties for the methane-steam reforming [Xu and Froment, 1989]

i	Reactions	Rate expressions	Heat of reaction at 298 K ΔH_R^0 (kJ/mol)	Equilibrium constant, K_{eqi}
1	$CH_4+H_2O=CO+3H_2$	$r_1=\dfrac{\dfrac{k_1}{P_{H_2}^{2.5}}\left(P_{CH_4}P_{H_2O}-\dfrac{P_{H_2}^3P_{CO}}{K_{eq1}}\right)}{(DEN)^2}$	206.1	$K_{eq1}=\exp\left[30.114-\dfrac{26,830}{T}\right]\times10^{-2}$
2	$CO+H_2O=CO_2+H_2$	$r_2=\dfrac{\dfrac{k_2}{P_{H_2}}\left(P_{CO}P_{H_2O}-\dfrac{P_{H_2}P_{CO_2}}{K_{eq2}}\right)}{(DEN)^2}$	−41.15	$K_{eq2}=\exp\left[-4.036+\dfrac{4,400}{T}\right]$
3	$CH_4+2H_2O=CO_2+4H_2$	$r_3=\dfrac{\dfrac{k_3}{P_{H_2}^{3.5}}\left(P_{CH_4}P_{H_2O}^2-\dfrac{P_{H_2}^4P_{CO_2}}{K_{eq3}}\right)}{(DEN)^2}$	164.9	$K_{eq3}=K_{eq1}\times K_{eq2}$

$DEN=1+K_{CO}p_{CO}+K_{H_2}p_{H_2}+K_{CH_4}p_{CH_4}+K_{H_2O}\cdot P_{H_2O}/P_{H_2}$

Table 2. Kinetic parameters for the methane-steam reforming [Xu and Froment, 1989]

Kinetic parameters	Pre-exponential terms, k_{i0}, K_{i0}	Activation energies or heats of chemisorptions, Ea, ΔH, kJ/mol	Units
k_1	4.225×10^{15}	240.1	kmol-bar$^{0.5}$/kg-cat/hr
k_2	1.955×10^{6}	67.13	kmol/kg-cat/hr/bar
k_3	1.020×10^{15}	243.9	kmol-bar$^{0.5}$/kg-cat/hr
K_{CO}	8.23×10^{-5}	−70.65	bar^{-1}
K_{H_2}	6.12×10^{-9}	−82.90	bar^{-1}
K_{CH_4}	6.65×10^{-4}	38.28	bar^{-1}
K_{H_2O}	1.77×10^{5}	88.68	-

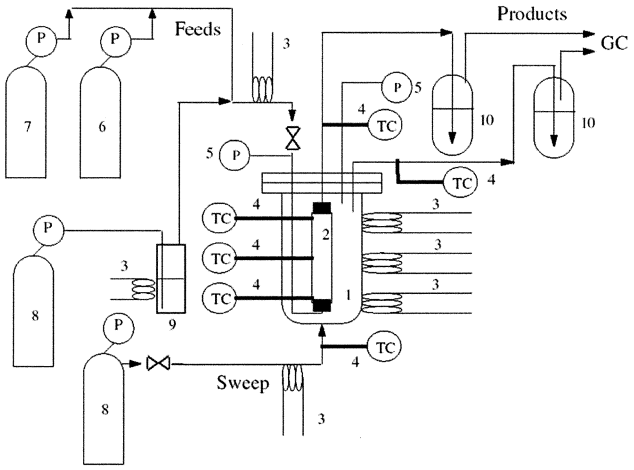

Fig. 1. A typical schematic presentation of an experimental system setting for HAMR.

1. Reactor
2. Membrane
3. Heaters
4. Thermocouples
5. Pressure gauges
6. CH_4
7. H_2
8. Inert gas
9. Water evaporator
10. Collector with condenser

is shown in Fig. 1, and more detailed one only for the reactor zone in Fig. 2. In Fig. 2 the interior of the membrane volume is signified by the superscript F, (feed-side), the exterior membrane volume signified by the superscript P, (permeate-side), and inside of the membrane is signified by the superscript m, (membrane-side). There are, of course, a number of potential reactor configurations. For example, 1) the adsorbent packed in the permeate-side of the membrane while the catalyst presented in the feed-side (HAMRP), 2) the adsorbent and the catalyst loaded together in the feed-side (HAMRF), 3) the catalyst packed in the permeate-side while the adsorbent packed in the feed-side, or 4) the catalyst and the adsorbent may only be loaded in the internal membrane. To simplify matters, in the development of the model we are assuming that external mass transfer resistances are negligible for the transport through the membrane, as well as for the reaction steps, and that internal diffusion limitations for the catalyst, and internal or external transport limitations are accounted by overall rate coefficients. Axially dispersed plug-flow conditions are assumed to prevail for both the interior and exterior membrane spaces, as well as ideal gas law conditions. Furthermore, commercial reformers are being operated under non-isothermal, non-adiabatic conditions in the range of temperature where hot-spots are not established within the reactor length. For instance,

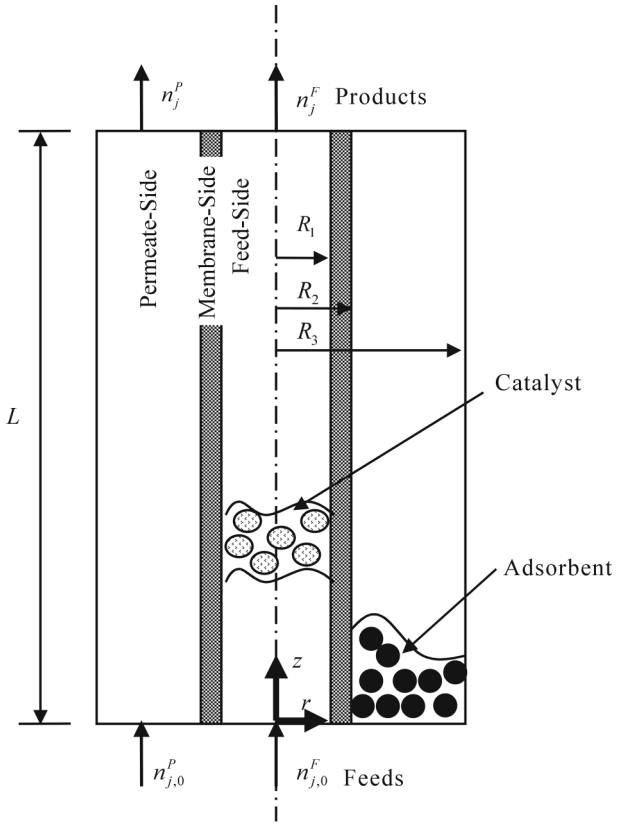

Fig. 2. Schematic diagram of HAMRP.

the reactor wall temperature for a commercial reformer varies from 973 K to 1,203 K, meanwhile the gas inlet temperature of 633 K and the out temperature of 1,066 K [Hyman, 1968]. In contrast with the operational conditions for commercial reformers, as seen in Fig. 1, the HAMR is operated under non-adiabatic, isothermal conditions by means of temperature profile control utilizing the three different temperature controllers attached on the reactor wall with measuring both the inlet and the outlet gas temperature. The HAMR system is assumed, furthermore, to operate under quasi-steady conditions with reaction/transport processes in the catalyst and transport properties through the membrane relaxing much faster than the slow changes in the adsorbent state due to saturation.

2-1. Membrane Inside, m

In our model of the HAMR reactor, we are mostly investigating commercially available membranes with Knudsen transport characteristics. Mass transfer through the porous membrane is described

through the following equation:

$$\frac{1}{R_g T}\frac{1}{r}\frac{d}{dr}\left[D_{je} r \frac{dP_j^m}{dr}\right]=0 \quad (6)$$

with boundary conditions: $r=R_1$; $P_j^m=x_j^F P^F$, $r=R_2$; $P_j^m=x_j^P P^P$

In Eq. (6), subscript j refers to species j. Superscripts m, F, P refer to the membrane-side, feed-side and permeate-side, respectively. The r is the coordination of the membrane reactor. R_1 and R_2 are the inside and outside radius of the membrane, respectively. P_j is partial pressure of species j. P^F and P^P are total pressure in the feed-side and permeate-side, respectively. x^F and x^P are mole fractions of the species j on the feed-side and permeate-side, respectively. D_{je} is effective pore diffusion coefficient. The effective pore diffusion coefficients can be estimated by the following relations [Froment and Bischoff, 1990]: $\frac{1}{D_{je}}=\sum_{i=1}^{N}\frac{1}{D_{j-ie}}\left(x_i^m-x_j^m\frac{N_i}{N_j}\right)+\frac{1}{D_{je}^K}$, where D_{je}^K is effective Knudsen diffusion coefficient, D_{j-ie} is binary molecular diffusion coefficient and N is flux.

2-2. Feed-Side, F

Taking the mass balance on the feed-side of the membrane reactor packed with methane-steam reforming catalyst leads to the following equations:

$$\frac{dn_j^F}{dz}=(2\pi R_1)\times\frac{1}{R_g T}\left[D_{je}\frac{dP_j^m}{dr}\right]_{r=R_1}+(1-\varepsilon^F)(\pi R_1^2)(\beta_{cat}\cdot\rho_{cat})(r_j^F) \quad (7)$$

If the inside of the membrane is packed with CO_2 removal adsorbents, Eq. (7) for CO_2 can be replaced by the following equation:

$$\frac{dn_{CO_2}^F}{dz}=(2\pi R_1)\times\frac{1}{R_g T}\left[D_{CO_2 e}\frac{dP_{CO_2}^m}{dr}\right]_{r=R_1}+(1-\varepsilon^F)(\pi R_1^2)(\beta_{cat}\cdot\rho_{cat})(r_{CO_2}^F) -(1-\varepsilon^F)(\pi R_1^2)(1-\beta_{cat})(\rho_{ads})(G_{CO_2}^F) \quad (8)$$

with initial conditions at z=0; $n_j^F=n_{j0}^F=(v_0^F x_{j0}^F P_0^F)/RT$

In Eq. (7) and Eq. (8), subscript 0 indicates the values at the entrance condition, which is constant, and j represents to H_2, CO, CO_2, CH_4 or H_2O. r_j^F is the rate of reaction occurring in the feed-side for j species as described from Eq. (1) to Eq. (5). R_1 is the inside radius of the membrane. ρ_{cat} and ρ_{ads} are the bulk density of catalysts and adsorbents, respectively, and the β_{cat} is the solid volume fraction occupied by catalysts ($\beta_{cat}=1$ when no adsorbent is present). ε^F is the bed porosity of the feed-side produced by catalyst, or catalyst together with CO_2 removal adsorbent packing. v is the volumetric flow rate. $G_{CO_2}^F$ is the rate of CO_2 adsorption described in following Eq. (9). The n_j^F is the molar flow rate of species j. The z is the axial position of the membrane reactor.

One may be able to find a number of approaches in the literature for describing $G_{CO_2}^F$ [Ding and Alpay, 2000a, b; Karger and Ruthven, 1992]. Ideally, one would like to account explicitly for both external and internal mass transport, and finite rates of adsorption. Such an approach goes beyond the scope of this preliminary investigation, however, in addition to the fact that there are currently no experimental high temperature transport/adsorption CO_2 data to justify this level of mathematical technical detail. Traditionally, in the modeling of adsorptive reactors simpler models have been utilized instead [Ding and Alpay, 2000a, b]. Two such models have received the most attention: (i) a model based on the assumption of an instantaneous local adsorption equilibrium (ILE) between the gas and the adsorbent phases [Ding and Alpay, 2000a, b; Park and Tsotsis, 2004], and linear driving force models (LDF), according to Karger and Ruthven [Karger and Ruthven, 1992] (see also 2003; Ding and Alpay, 2000a, b) G_{CO2}^F is described by the following expression:

$$G_{CO_2}^F=k(C_{CO_2}^{eq,F}-C_{CO_2}^F) \quad (9)$$

where $C_{CO_2}^{eq,F}$ is the adsorption equilibrium CO_2 concentration on the adsorbent, $C_{CO_2}^F$ is CO_2 concentration in solid-phase, and k is a mass transfer parameter which lumps together the effects of external and intra-particle mass transport and the sorption processes, and which, as a result, is often a function of temperature and pressure [Ding and Alpay, 2000b] - though, typically, in modeling is taken as temperature and pressure independent. Ding and Alpay [2000b] reported that the k is the same value of 360 hr^{-1} at 673 K and 4.4 bar for hydrotalcite. In calculation of $C_{CO_2}^{eq}$, According to Ding and Alpay [2000b] for CO_2 adsorption on potassium promoted hydrotalcite, the CO_2 adsorption on this adsorbent follows Langmuir adsorption isotherm both under dry and wet conditions, described by the following equation:

$$C_{CO_2}^{eq}=\frac{m_{CO_2} b_{CO_2} P_{CO_2}^F}{1+b_{CO_2} P_{CO_2}^F} \quad (10)$$

where m_{CO_2} is the total adsorbent capacity, and b_{CO_2} is the adsorption equilibrium constant. The b_{CO_2} can be estimated by the van't Hoff equation [Ding and Alpay, 2000b]:

$$b_{CO_2}=b_{CO_2}(T_0)\exp(-\Delta H_a/R(1/T-1/T_0)) \quad (11)$$

where ΔH_a is heat of adsorption and T_0 is 298 K. The heat of adsorption ΔH_a under wet conditions for a region of temperatures from 481 to 753 K was calculated to be −17 kJ/mol [Ding and Alpay, 2000a]. Values for b_{CO_2} and m_{CO_2} at 753 K are equal to 19.3 bar^{-1} and 0.58 mol/kg for hydrotalcite, respectively [Ding and Alpay, 2000b]. In this paper we will assume that the applicability of the above relationship extends to 873 K. In calculation of $G_{CO_2}^{eq}$, we will utilize the data reported by Ding and Alpay [2000a, b] for CO_2 adsorption on a potassium promoted hydrotalcite.

Pressure drop in the feed-side packed with catalyst and/or adsorbent can be described by the Ergun equation [Ergun, 1952]:

$$\frac{dP^F}{dz}=-K_D u_2^F-K_v(u_z^F)^2 \quad (12)$$

with initial condition at z=0; $P^F=P_0^F$

where K_D and K_v are parameters contributed by viscous and kinetic pressure drops as follows:

$$K_D=150\frac{\mu_g[\lambda_s(1-\varepsilon_b)]^2}{d_p^2\varepsilon_b^3} \quad (13)$$

$$K_v=1.75\frac{\lambda_s(1-\varepsilon_b)\rho_p}{d_p\varepsilon_b^3} \quad (14)$$

In Eq. (12), Eq. (13) and Eq. (14), u_z the superficial velocity, μ_g is gas viscosity, ρ_g is gas density, and d_p is particle diameter.

2-3. Permeate-side, P

Permeate gases are swept away by inert sweep gas, which is water vapor, at the entrance of the permeate-side of the membrane reactor. To improve the CO_2 removal, the permeate-side or feed-side of

the membrane reactor is packed with CO_2 removal adsorbent. Assuming no reactions occur, the mass balance on the permeate-side of the membrane reactor becomes:

$$\frac{dn_j^P}{dz} = -(2\pi R_2)\times\frac{1}{RT}\left[D_{je}\frac{dP_j^m}{dr}\right]_{r=R_2} \tag{15}$$

For the same reason in Eq. (8), the above Eq. (15) became the following, Eq. (16):

$$\frac{dn_{CO_2}^P}{dz} = -(2\pi R_2)\times\frac{1}{RT}\left[D_{CO_2e}\frac{dP_{CO_2}^m}{dr}\right]_{r=R_2} - (1-\varepsilon^P)(\pi R_3^2-\pi R_2^2)(\rho_{ads})(G_{CO_2}^P) \tag{16}$$

with initial conditions: z=0; $n_j^P=n_{j0}^P=(v_0^P x_{j0}^P P_0^P)/RT$

where ε^P is the porosity in the permeate-side produced by only CO_2 removal adsorbent.

Pressure drop in both the permeate-side packed with catalyst and/or adsorbent can be again described by the Ergun equation [Ergun, 1952]:

$$\frac{dP^P}{dz} = -K_D u_z^P - K_v (u_z^P)^2 \tag{17}$$

with initial condition at z=0; $P^P=P_0^P$

where K_D and K_v are described in the Eq. (13) and Eq. (14):

The reactor conversion (based on methane, typically the limiting reagent) is defined by the following equation:

$$X_{CH_4} = \frac{n_{CH_4,0}^F - (n_{CH_4}^F + n_{CH_4}^P)}{n_{CH_4,0}^F} \tag{18}$$

where $n_{CH_4}^F$ and $n_{CH_4}^P$ are the methane molar flow rates of the reactor feed-side and permeate-side, respectively.

The product hydrogen yield is defined by the following equation:

$$Y_{H_2} = \frac{1}{4}\times\frac{n_{H_2}^F + n_{H_2}^P}{n_{CH_4,0}^F} \tag{19}$$

where $n_{H_2}^F$ and $n_{H_2}^P$ are the hydrogen molar flow rates of the reactor feed-side and permeate-side, respectively.

3. Dimensionless Model Equations

Equations from Eq. (1) to Eq. (17), and their boundary conditions and initial conditions can be written in dimensionless equations by defining the following dimensionless parameters and variables:

$$\eta = \frac{z}{L}\quad \omega = \frac{\ln\xi}{\alpha}\quad \xi = \frac{r}{R_1}\quad \alpha = \ln\left(\frac{R_2}{R_1}\right)\quad \Psi_j^m = \frac{P_j^m}{P_0^F}\quad x_j^F = \frac{P_j^F}{P_0^F}\quad x_j^P = \frac{P_j^P}{P_0^P}$$

$$\theta_{CO_2}^F = \frac{C_{CO_2}^F}{m_{CO_2}}\quad \theta_{CO_2}^P = \frac{C_{CO_2}^P}{m_{CO_2}}\quad \psi^F = \frac{P^F}{P_0^F}\quad \psi^P = \frac{P^P}{P_0^F}\quad \psi_0^P = \frac{P_0^P}{P_0^F}\quad y_j^F = \frac{n_j^F}{n_0^F}$$

$$y_j^P = \frac{n_j^P}{n_0^F}\quad \theta_{CO_2}^{eq,F} = \frac{C_{CO_2}^{eq,F}}{m_{CO_2}} = \frac{b'_{CO_2}x_{CO_2}^F\psi^F}{1+b'_{CO_2}x_{CO_2}^F\psi^F}$$

$$\theta_{CO_2}^{eq,P} = \frac{C_{CO_2}^{eq,P}}{m_{CO_2}} = \frac{b'_{CO_2}x_{CO_2}^P\psi^P}{1+b'_{CO_2}x_{CO_2}^P\psi^P}\quad b'_{CO_2} = b_{CO_2}\times P_0^F\quad \delta_j = \frac{D_{je}}{D_{H_2Oe}}$$

$$Q = \frac{(2\pi\cdot L)(D_{H_2Oe})}{v_0^F}\quad Da = \frac{(1-\varepsilon^F)(k_1)(\beta_{cat}\cdot\rho_{cat}\cdot V^F)}{n_0^F}$$

$$Re^F = \frac{\rho_g^F\cdot u_z^F(2\cdot R_1)}{\mu_g^F}\quad Re^P = \frac{\rho_g^P\cdot u_z^P\cdot 2(R_3-R_2)}{\mu_g^P}\quad \Gamma^F = \frac{L}{2\cdot R_1}$$

Table 3. Separation factors calculated from relative Knudsen diffusion coefficients

Components	Molecular weights, Mw_i	Separation factor, calculated, $\delta_j=D_{je}/D_{water,e}$
H_2	2.02	2.99
CH_4	16.04	1.06
H_2O	18.02	1.0
CO	28.01	0.80
CO_2	44.01	0.64

$$\Gamma^P = \frac{L}{2(R_3-R_2)}\quad Ha^F = \frac{(1-\varepsilon^F)(1-\beta_{cat})(k\cdot m_{CO_2}\cdot\rho_{ads}\cdot V^F)}{n_0^F}$$

$$Ha^P = \frac{(1-\varepsilon^P)(k\cdot m_{CO_2}\cdot\rho_{ads}\cdot V^P)}{n_0^F}\quad \prod_j^F = f(x_j^F)$$

$$K^F = \frac{K_D^F\cdot\mu_g^F + K_v^F\cdot\mu_g^F\cdot u_z^F}{\rho_g^F P_0^F}\quad K^P = \frac{K_D^P\cdot\mu_g^P + K_v^P\cdot\mu_g^P\cdot u_z^P}{\rho_g^P P_0^P}$$

where Da is a modified Damkohler number, reciprocal of Q/α is a modified Peclet number, Re is a Reynolds number, Ha is a modified Hatta number, and Γ is a geometric factor of the reactor shape. R_1 and R_2 are the inside and the outside radius of the membrane, respectively, and R_3 is the radius of the HAMR. The subscript 0 indicates the condition at the entrance of the HAMR, which is constant. δ_j is the separation factor relative to the effective pore diffusion coefficient for water vapor. The experimentally observed binary separation factors for such a porous alumina membrane closely follow the ratios of Kudsen diffusion, $\delta_{j-i}=D_{je}/D_{ie}\cong\sqrt{Mw_i/Mw_j}$ as ideal binary separation factors. Values for the ideal separation factor are summarized in Table 3.

Now, dimensionless equations for the membrane reactors become:

3-1. Membrane-Side, m

$$\frac{d^2\Psi_j^m}{d\omega_2} = 0;\ \text{at } \omega=0;\ \Psi_j^m = x_j^F\psi^F \text{ and } \omega=1;\ \Psi_j^m = x_j^P\psi^P \tag{20}$$

3-2. Feed-Side (Tube-Side), F

$$\frac{dy_j^F}{d\eta} = (\delta_j)\left(\frac{Q}{\alpha}\right)\left[\frac{d\Psi_j^m}{d\omega}\right]_{\omega=0} + Da\times\prod_j^F;\ \text{at } \eta=0;\ y_j^F = y_{j0}^F = x_{j0}^F \tag{21}$$

$$\frac{d\psi^F}{d\eta} = -(K^F)(\Gamma^F)(Re^F) \qquad \text{at } \eta=0;\ \psi^F=1 \tag{22}$$

when the feed-side is packed with CO_2 removal adsorbent, Eq. (13) can be expressed as:

$$\frac{dy_{CO_2}^F}{d\eta} = (\delta_{CO_2})\left(\frac{Q}{\alpha}\right)\left[\frac{d\Psi_{CO_2}^m}{d\omega}\right]_{\omega=0} + Da\times\prod_{CO_2}^F - Ha^F\times(\theta_{CO_2}^{eq,F} - \theta_{CO_2}^F) \tag{23}$$

3-3. Permeate-Side (Shell-Side), P

$$\frac{dy_j^P}{d\eta} = -(\delta_j)\left(\frac{Q}{\alpha}\right)\left[\frac{d\Psi_j^m}{d\omega}\right]_{\omega=1};\ \text{at } \eta=0;\ y_j^P = y_{j0}^P = \Phi x_{j0}^P\psi^P \tag{24}$$

$$\frac{d\varphi^P}{d\eta} = -(K^P)(\Gamma^P)(Re^P) \qquad \text{at } \eta=0;\ \psi^P = \psi_0^P \tag{25}$$

if the permeate-side is packed with CO_2 removal adsorbent, Eq. (15) becomes:

$$\frac{dy^P_{CO_2}}{d\eta} = -(\delta_{CO_2})\left(\frac{Q}{\alpha}\right)\left[\frac{d\Psi^m_{CO_2}}{d\omega}\right]_{\omega=1} - Ha^P \times (\theta^{eq,P}_{CO_2} - \theta^P_{CO_2}) \quad (26)$$

4. Reactor Simulation

In order to compare the behavior of four different types of reactors, a classical plug-flow reactor, a conventional membrane reactor, and two different types of HAMR, one for which the catalyst and adsorbent are packed together in the feed-side, termed HAMRF, and another for which the catalyst is packed in the feed-side and the adsorbent is packed in the permeate-side, termed HAMRP, utilizing the developed model equations, as an example, these model equations were applied to methane-steam reforming. In this preliminary work, a cylindrical porous ceramic membrane was used in which the actual perm-selective layer existed on the innermost surface. The interior space of the ceramic membrane was packed with methane-steam reforming catalysts, e.g., supported nickel pellets. Feed gas mixtures and the sweep gas were introduced on the bottom of the feed-side and permeate-side of the membrane reactor, respectively.

Using reaction conditions and parameters summarized in Table 4 together with the values in Tables 1, 2 and 3, we performed rigorous calculations to assess the feasibility of the HAMR systems. The catalyst contact time for feed gas was 1.0 g-cat-hr/mole. Typical mole ratio of the feed gas mixture was 3.0 H_2O : 1.0 CH_4 : 0.10 H_2. For the system to be more realistic, we bench marked size and characteristics of a commercial asymmetric porous tubular type γ-alumina membrane (Membralox™ produced by U. S. Filter). According to the preliminary mass transfer experiment utilizing H_2 and CH_4 as probes, the pore size of the Membralox™ membrane was in the Knudsen diffusion regime. It had inside radius of 0.350×10^{-3} m and thickness of 5.0×10^{-5} m. The length of the membrane was 0.30 m. The feed-side pressure was varied from 3 to 10 atm, while the permeate-side was kept constant at 2 atm. Values of the Q/α were over 3.08. The inert gas sweep ratio was 3.0 in the permeate-side. Hatta number is about 81.

Table 4. Conditions and parameters for the HAMRs

Conditions or parameters	Values	Units
Feed-side:		
Total molar flow rate, n^F_0	4.10	moles/hr
Mole ratio, $n^F_{CH4,0} : n^F_{H2O,0} : n^F_{H2,0}$	3.0 : 1.0 : 0.1	moles/hr
Weight of catalyst, W_{cat}	4.10	g
Volume for HAMRF, V^F	3.10×10^{-3}	m^3
Volume for HAMRP, V^F	1.15×10^{-5}	m^3
Temperature, T	800-1,000	K
Pressure, P^F_0	3.0-10.0	bar
Permeate-side:		
Volume for HAMRF, V^P	1.15×10^{-5}	m^3
Volume for HAMRP, V^P	3.10×10^{-3}	m^3
Inert gas sweep ratio, v^P_0/v^F_0	3.0	dimensionless
Temperature, T	800-1,000	K
Pressure, P^P_0	2	bar
Parameters:		
b for CO_2 at 753 K	19.3	bar^{-1}
m for CO_2 at 753 K	0.58	moles/kg
k	360	hr^{-1}
Bulk density of hydrotalcite, ρ_{ads}	1,563	kg/m^3
Bulk density of catalyst, ρ_{cat}	139	kg/m^3
Viscosity of gas, μ_g	8.3×10^{-9}	Pa-hr
Solid volume fraction for catalyst, β_{cat}	0.03	dimensionless
Hatta number for HAMRF, Ha^F	81	dimensionless
Hatta number for HAMRP, Ha^P	81	dimensionless
Porosity, ε^P, ε^F	0.67	dimensionless
Q/α	over 3.08	dimensionless

RESULTS AND DISCUSSIONS

1. Calculations for a Conventional Tubular Type Packed Bed Plug Flow Reactor (PFR)

In order to compare the conversion and dimensionless molar flow rate values for the different types of the membrane reactor modes of operations, we also have calculated the values for the conventional tubular type packed bed plug flow reactor (PFR); these are actually equilibrium values, undergoing methane-steam reforming as reference values. This PFR condition corresponds to Q/α equals to zero in the model equations for the catalytic packed bed membrane reactors.

Fig. 3 shows the calculation results for the performance of the conventional tubular type PFR against the dimensionless length of the PFR. The dotted line indicates reaction conversions for methane, and the solid line depicts dimensionless molar flow rates for reactants CH_4, H_2O and products H_2, CO_2 and CO. The operating conditions for the PFR used in this calculation are pressure of 3 atm and temperature of 873 K. The feed mole ratio introduced into the PFR was 3.0 H_2O : 1.0 CH_4 : 0.10 H_2. As shown in Fig. 3, the reaction conversions for methane and all of the dimensionless molar flow rates asymptotically reach equilibrium values at a reactor length of 5%. The equilibrium conversion for methane is 54%, which is the maximum allowable conversion in the PFR at the given conditions. This level of equilibrium methane conversion leads to the maximum amount of hydrogen production.

2. Calculation for a Packed Bed Catalytic Membrane Reac-

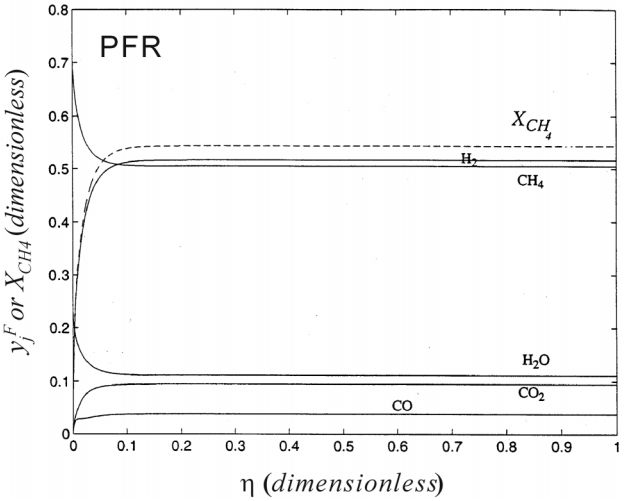

Fig. 3. Plots on the dimensionless molar flow rate and the methane conversion against dimentsionless length for PFR.

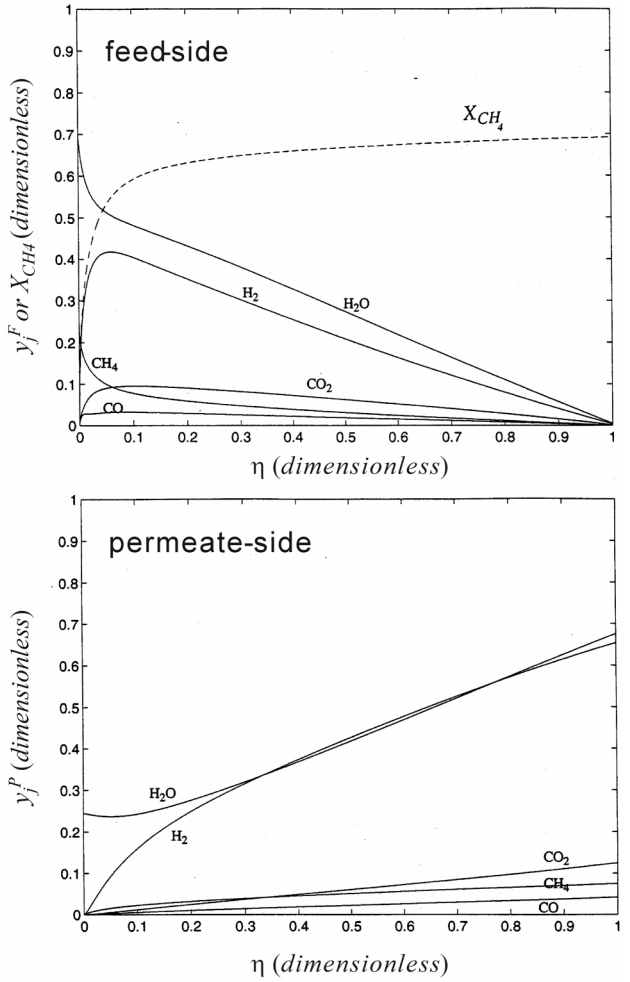

Fig. 4. Plots on the idmensionless molar flow rate and the methane conversion against dimensionless length for MR.

tor (MR)

Fig. 4 shows calculation results for the performance of the packed bed catalytic porous ceramic membrane reactor (MR) for both the feed-side and the permeate-side. The operating conditions of the MR for the feed-side are the same conditions as that of the PFR. The conditions for the permeate-side are pressure of 2 atm and temperature of 873 K. All other conditions for both the feed-side and the permeate-sides are summarized in Table 4. Again, the dotted line shows the reaction conversion for methane and the solid lines depicts the dimensionless molar flow rates of chemical species. At the end of the MR, the observed reaction conversion for methane is 69%, while the conversion is only 54% at the end of the PFR. Clearly, there is a 15% conversion gain by means of the MR.

In the feed-side, from the entrance of the MR up to the reactor length of 5%, the reaction conversions and the molar flow rates quickly reach near equilibrium values. The reason is that the value for the second term in the right-hand side of Eq. (21), which represents the level of the rate of the methane-steam reforming reaction, is greater than the level of the contribution term for the rate of mass transfer. From the entrance up to the 5% length for the MR, the feed-side of the MR shows as same reactor behavior as we observed in the PFR.

Now, from the length of 5% to the end of the feed-side of the MR, the first term in the right-hand side of Eq. (21), which is the level of the mass transfer through the porous membrane, becomes more important. Over the length of 5%, the change for the dimensionless molar flow rates becomes slower than that observed in the early stage of the feed-side length, i.e., from the entrance to the length of 5%. This is because the level of amounts of all species already reaches near equilibrium. As shown in Fig. 4, over a length of 5% in the feed-side, the dimensionless molar flow rates for all products and reactants still gradually decrease with an increase in the tube length, while the reaction conversion for methane increases. This is the typical membrane reactor behavior when compared with the conventional reactor behavior. Note that this phenomenon, the continuous increasing for the methane conversion over the length of 5%, can be explained by equilibrium-shift. Compared to the results in Fig. 3 for the PFR, it is obvious that the removal of the products H_2, CO, CO_2 from the feed-side of the PBMR leads to a 15% gain for the methane conversion by the equilibrium-shift in the forward reactions.

Removed species from the feed-side appear in the permeate-side. In this calculation, water vapor has been used as an inert sweep gas. This is why the amount of the water vapor is relatively very high in

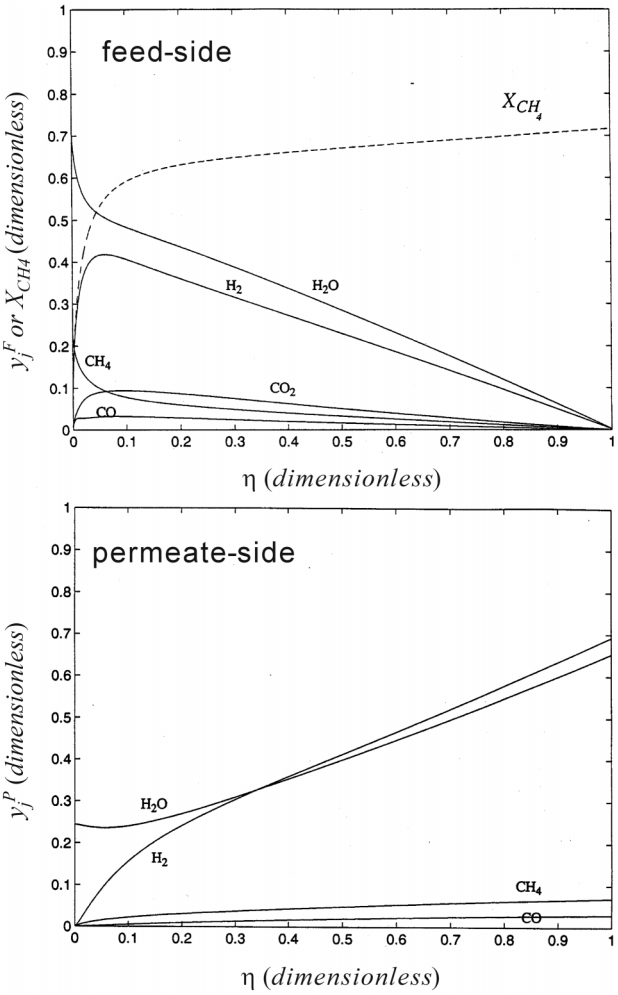

Fig. 5. Plots on the dimensionless molar flow rate and the methane conversion against dimensionless length for HAMRP.

the permeate-side. However, for practical purposes, water vapor is better to be replaced by hydrogen gas. About 10% of total amount for feed methane has appeared in the permeate-side without any further reaction. All species have been accumulated in the permeate-side. Compared to the amount of hydrogen production in the PFR, 27% more hydrogen has been produced in the MR by enhanced equilibrium-shift.

3. Calculations for an HAMR Packed with CO_2 Removal Adsorbent in the Permeate-Side (HAMRP)

Fig. 5 shows the calculation results of the packed bed catalytic porous ceramic membrane reactor integrated with CO_2 removal adsorbent in the permeate-side (HAMRP). The HAMRP has been operated with the same MR conditions. The only difference from the MR is that the permeate-side of the HAMRP is packed with the CO_2 removal adsorbents. By means of this byproduct CO_2 removal adsorbent system, we have expected to reduce the partial pressure of CO_2 in the permeate-side near zero. In the Eq. (25), the value for the Hatta number, Ha, is about 40 times greater than that for the product of separation factor, δ_j, and Q/α for CO_2. Therefore, CO_2 penetrating from the feed-side to permeate-side through the membrane is quickly removed by the adsorbent system. Consequently, the value of concentration for CO_2 approaches to near zero. The high level of the mass-transfer driving force across the porous membrane has been enhanced by maintaining the low level of the CO_2 partial pressure in the permeate-side. Finally, the forward reactions have reinforced by the equilibrium-shift. A methane conversion of 72% is obtained by using HAMRP. This level of the methane conversion is about 18% higher than the level of the equilibrium methane conversion calculated in the PFR, and 3% higher than the level of the methane conversion observed in the MR. In terms of hydrogen production using the HAMRP, as of Fig. 5, a 35% gain has been obtained compared to the level of the amount for the equilibrium production estimated in the PFR.

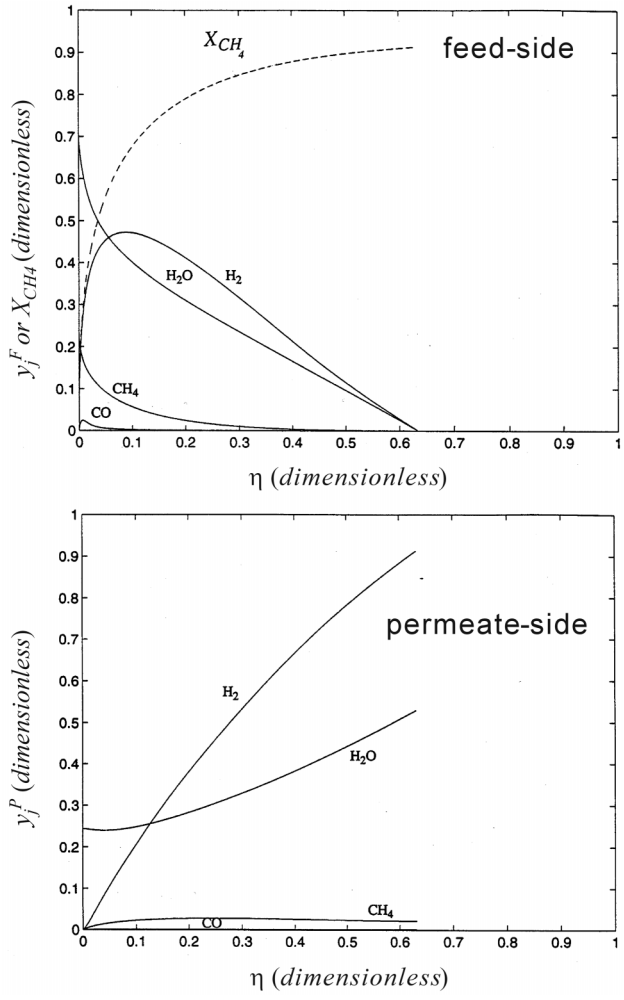

Fig. 6. Plots on the dimensionless molar flow rate and the methane conversion against dimensionless length for HAMRF.

4. Calculations for an HAMR Packed with CO_2 Removal Adsorbent in the Feed-Side (HAMRF)

Compared to the results of the MR and/or the HAMRP, as shown in Fig. 6, very significant changes have been observed in the ceramic membrane reactor packed with both the CO_2 removal adsorbent and the catalyst in the feed-side (HAMRF). The same HAMRP operating conditions have been used for the HAMRF. The only difference is, between the conditions for the HAMRP and the HAMPF mode of operations, the volume of the membrane inside. In the case of the HAMRF type reactor mode of operation, the volume of the membrane inside was 3.0×10^{-3} m^3 instead of 1.15×10^{-5} m^3 of the membrane inside volume for the HAMRP. This volume provides enough space for additional CO_2 removal adsorbent packing. Solid volume fraction of catalyst, β_{cat}, is 0.03.

The calculation results for both the feed-side and the permeate-side have been plotted against the dimensionless length of the HAMRF. In the feed-side of the HAMRF, the dimensionless molar flow rate for hydrogen production shows a maximum value at the length of 8%. Remarkably, after passing the maximum value, the dimensionless molar flow rate in the feed-side of the HAMRF is much more quickly decreasing than that observed in the other reactor modes of operations up to about the tube length of 63%. This is similar behavior commonly observed in adsorption-enhanced reformers proposed by others [Lee et al., 2004; Ding and Alpay, 2000a, b; Han and Harrison, 1994; Prasad and Elnashaie, 2004; Xiu et al., 2002, 2003]. In the HAMRF, 100% of all chemical species in the feed-side has been removed at this reactor length. Compared to the other reactor modes of operations, it can be explained that CO_2 has been quickly depleted and therefore no longer exists in the both feed-side and/or the permeate-side of the HAMRF due to the relatively very fast CO_2 removal in the feed-side. Consequently, the equilibrium has much more quickly shifted toward the forward reactions. As a result, the reaction conversion for methane in the HAMRF very quickly reaches 93% together with the gain of hydrogen yield of 82% compared to the yield observed in the PFR.

There is about 4% unreacted methane loss from the fee-side appearing in the permeate-side. It seems that the HAMR system requires tighter pore size membrane to prevent the loss of unreacted feed from the fee-side. However, this improvement in the reactor performance is very significant. Note that the level of the methane conversion observed in the HAMRF is 39% higher than that in the PFR, i.e., equilibrium methane conversion. In addition, compared to the results on the MR, 43% more hydrogen has been produced and accumulated in the permeate-side of the HAMRF. By the calculation results, it can be proposed that, presumably, in order to produce purified hydrogen, the water vapor sweep in the permeate-

side of the HAMRF system had better be replaced by the hydrogen gas sweep. Also, installing a water condenser on the exit of the permeate-side can be an alternative means of the removal of water vapor.

5. Effect of Pressure and Temperature on the Various Reactor Types

In Fig. 7, the calculated reaction conversions for methane and yields for hydrogen have been plotted against temperature and pressure as a parameter. In this calculation, range of conditions for the feed-side covers temperature from 823 K to 1,073 K and pressure from 3 bar to 10 bar. All other conditions are the same condition as the MR. The dashed line illustrates the calculation results on the PFR in equilibrium mode of operation, the solid line describes the results on the HAMRP, the dotted line depicts the results on the HAMRF, and the dashed-dot line shows the results on the MR. As shown in Fig. 7, significant improvements in methane conversion and hydrogen yield have been achieved by the HAMRF, HAMRP and/or MR mode of operations over the PFR mode of operation.

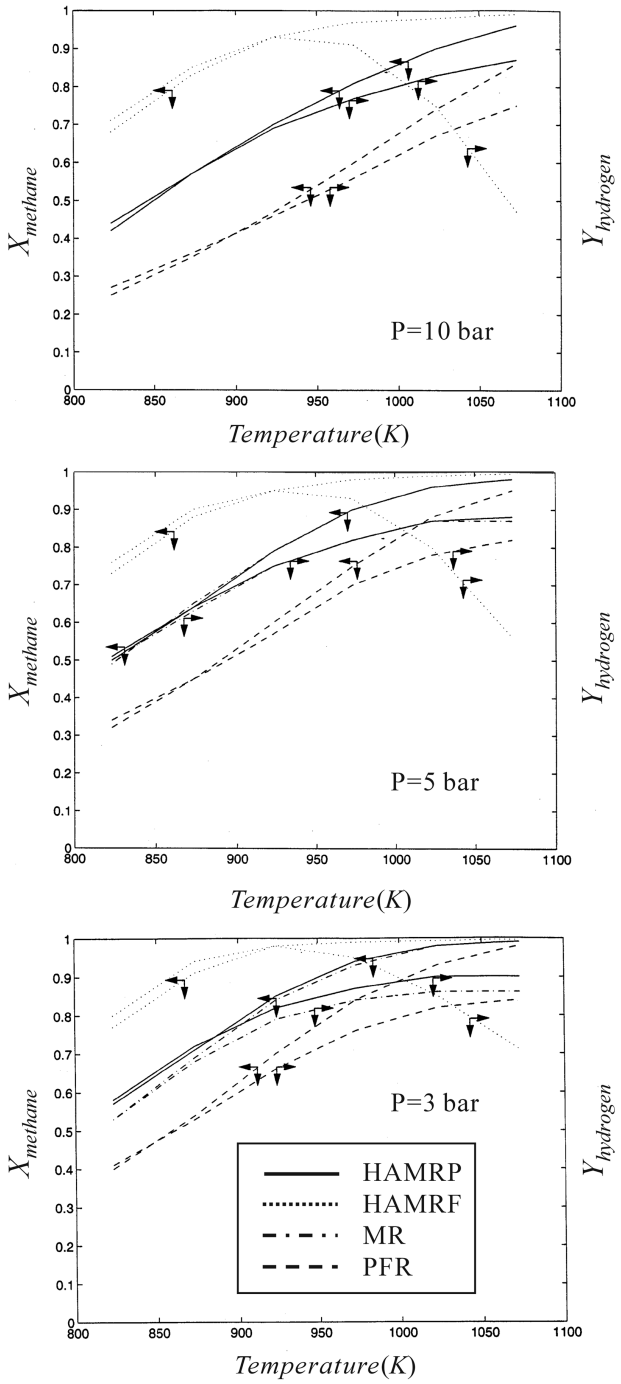

Fig. 7. Plots on the methane conversion and hydrogen yield as a function of temperature, pressure as a parameter for different reactor types.

In the PFR mode of operation, both the conversion of methane and the yield of hydrogen have increased when the temperature increases. As summarized in Table 1, heat of overall reaction for the methane-steam reforming has reported +164.9 kJ/mol. The positive value of the heat of reaction indicates that the reforming is endothermic. In the PFR mode of operation, low pressure and high temperature for the system favor the forward reactions. In addition, as well known, high steam ratios promote the high reforming conversion, but it requires additional heating cost; meanwhile, lower steam ratio runs the risk of carbon deposition within the PFR [Froment and Bischoff, 1990; Xu and Froment, 1989].

As shown in Fig. 7, obviously, the performance of the PFR can be drastically improved by MR, HAMRP or HAMRF modes of operations by the enhanced equilibrium-shift and CO_2 removal. In comparison between the MR and HAMRP, there is no remarkable improvement over the entire ranges of the calculations. This is because, for the CO_2 removal in the HAMRP mode of operation, the membrane acts as a sort of mass transfer barrier. The HAMRF shows the highest hydrogen production yield below a temperature near 1,000 K. In relatively high pressure range, for the HAMRF, the conversions for methane have decreased because more methane has been removed from the feed-side without reaction. The yields of hydrogen show maximum values upon increasing temperature. Over the temperature range showing the maximum values for the hydrogen yields, the level of the rate of mass transfer for methane across the membrane becomes higher, i.e., in the case of contribution of the first term in the right-hand side of the Eq. (21) becomes greater, than the level of the rate of reaction. Under this situation, more reactant methane has been removed from the feed-side to the permeate-side without reaction, and consequently the yield of hydrogen decreases.

Overall, among the four different modes of operations, the HAMRF mode of operation has shown the best performance. This configuration combines the adsorptive reactor proposed by others [Ding and Alpay, 2000a, b; Han and Harrison, 1994; Lee et al., 2004; Xiu et al., 2002, 2003] and *in situ* H_2 purifications by means of membrane separations. Produced H_2 has been enriched in the permeate-side of the HAMRF mode of operation. In addition, there is still a great chance of reducing volume of the feed-side by means of introducing CaO as an CO_2 removal adsorbent instead of the potassium promoted layered-double hydrotalcite adsorbent, because the CO_2 removal capacity of the CaO adsorbent is about five to ten times higher compared to that for potassium promoted layered-double hydrotalcite. Optimum conditions for the HAMRF mode of operation are temperature of near 900 K, and pressure of 3 atm. In comparison, commercial reformers have been operated with temperature of over 1,000 K, pressure of 20-30 atm and steam to hydrocarbon ratio of 2.4 to 4.0 [Elnashaie et al., 1990; Froment and Bischoff,

1990; Xu and Froment, 1989]. Indeed, by means of introducing the membrane and the CO_2 removal adsorbent system, the severe operation conditions for the methane steam reformer can potentially be drastically reduced into the mild operation conditions. Moreover, the PFR and conventional MR performances can also be greatly improved by utilizing the HAMRF. In HAMRP mode of operation utilizing potassium promoted layered-double hydrotalcite as a high temperature CO_2 adsorbent suitable for low temperature regeneration, a continuous operation with a single HAMRP is possible by means of introducing a continuous pulse-type or a sinusoidal-type sweep gas in permeate-side of the HAMRP. In this way, adsorbed CO_2 is periodically being regenerated. These changes are the areas of interest where significant energy savings are to be obtained. However, as mentioned earlier, there is still a big challenge to this work--finding a proper range of membrane pore size. As of the calculation results, there is somewhat of a reactant methane loss by penetrating through the porous membrane. It seems that there is still a strong chance of improving the performance of the HAMR if one uses a tighter membrane than the commercial membrane, which we used in this calculation. In this way, loss of reactant methane can be prevented, while only the products CO_2 and hydrogen are permeating through the membrane. In addition, preliminary experiments have revealed that one of the optimal configurations for the HAMR systems is the catalyst packed in the permeate-side while the adsorbent is in the feed-side. In this way, both heating of the catalyst and adsorption capacity of CO_2 are greatly improved by introducing relatively colder seep gas into the entrance of the feed-side.

CONCLUSIONS

We have investigated a novel reactor system, termed the hybrid adsorbent-membrane reactor (HAMR), for hydrogen production undergoing methane steam reforming. The HAMR combines the reaction and membrane separation steps (i.e., MR) incorporated with adsorption on the membrane feed-side (i.e., HAMRF) or permeate-side (i.e., HAMRP). This HAMR system is of potential interest to pure hydrogen production for fuel cells for various mobile and stationary applications. The reactor characteristics have been investigated in the ranges of temperature, pressure and other experimental conditions relevant to the aforementioned applications and compared with the behavior of the traditional packed-bed reactor, (i.e., PFR), a conventional membrane reactor, (i.e., MR). Among the tested reactors, the HAMR outperforms all the other more conventional reactor systems. In the HAMRF mode of operation, the conversion of the reactant methane and yield of the product hydrogen are nearly 100% and 98%, respectively--even milder conditions compared to the conventional reformer conditions. These are great improvements over the conventional methane steam reformers.

By means of introducing a CO_2 removal adsorbent system into the conventional MR, there are great chances of improving the performance of the conventional methane-steam reformers as well as conventional membrane reactors, producing hydrogen-rich gas stream, reducing the hostile operation conditions of the other more conventional reactors, reducing the cost of the reformer operation and reducing the cost of product purification, and potentially meeting the product purity requirements for fuel cell operation. Moreover, the price of metallic Pd or Pd-alloy membrane reactor can be greatly reduced if the expensive novel metal membrane is replaced by a cheap ceramic membrane. In this way, the fuel-cell grade purified hydrogen can be economically produced with the HAMR.

Finally, the downside of the HAMR systems: similarly to the adsorptive reactors, they require regeneration of the spent adsorbent, and for continuous operation they may require a dual reactor system, where one of the reactors is in operation while the other reactor is being regenerated. For practical purposes, to realize continuous modes of operations on these HAMRF or HAMRP systems, at least two identical reactors are required such as the pressure swing adsorption (PSA) or adsorptive reactor processes. In comparison to the adsorptive reactor, the major advantage of HAMRP is that the membrane can separate catalyst and adsorbent. In future publications, we will provide experimental validation of the HAMR system, solve simultaneously with energy conservation equation for non-isothermal operation of the HAMR to be more realistic, and extend the research to compare with the performance of the adsorptive reactor system as a competitive system of the HAMR system.

ACKNOWLEDGMENT

Thank you very much to Prof. Theodore T. Tsotsis of the Department of Chemical Engineering at the University of Southern California for his valuable discussions on this work.

NOMENCLATURE

b : parameter for Langmuir equation [bar^{-1}]
C : concentration [$moles/m^3$]
$C_{CO_2}^{eq}$: solubility of CO_2 in adsorbent [$moles/m^3$]
Da : modified Damkohler number [dimensionless]
D_{je} : effective pore diffusion coefficient [m^2/hr]
D_{CS} : cross section [m]
G_{CO_2} : rate of CO_2 adsorption [mole/kg/hr]
ΔH_R : heat of reaction [kJ/mol]
Ha : modified Hatta number [dimensionless]
k : mass transfer coefficient [hr^{-1}]
m : parameter for Langmuir equation [moles/kg]
n_j : molar flow rate [moles/hr]
P : pressure [bar]
Q/α : reciprocal of modified Peclet number [dimensionless]
r_j : rate of reaction [moles/kg/hr]
r_p : pore radius of membrane [m]
R_1 : inside radius of membrane [m]
R_2 : outside radius of membrane [m]
R_3 : radius of the reactor permeate-side [m]
R_g : ideal gas constant [m^3-bar/mole/K]
Re : Reynolds number [dimensionless]
T : absolute temperature [K]
u_z : z-directional superficial velocity [m/hr]
x_j : mole fraction [dimensionless]
X_{CH_4} : methane conversion [dimensionless]
y : dimensionless molar flow rate [dimensionless]
Y_{H_2} : hydrogen yield [dimensionless]

Greek Letters

α : dimensionless parameter [dimensionless]

β : volume fraction of solid in catalyst and adsorbent mixture [dimensionless]
δ : separation factor [dimensionless]
ε : porosity [dimensionless]
η : dimensionless length [dimensionless]
ρ : density [kg/m$_3$]
τ : tortuosity [dimensionless]
ω : dimensionless parameter [dimensionless]
ξ : dimensionless radius [dimensionless]
ψ : dimensionless pressure [dimensionless]
Ψ : dimensionless pressure [dimensionless]

Subscripts

0 : entrance condition
ads : adsorbent
cat : catalyst
eq. : equilibrium
i : ith chemical reaction in Table 1
j : chemical species

Superscripts

ads : adsorbent
cat : catalyst
eq. : equilibrium
m : membrane-side
F : feed-side
P : permeate-side

REFERENCES

Choi, Y. and Stenger, H. G., "Water Gas Shift Reaction Kinetics and Reactor Modeling for Fuel Cell Grade Hydrogen," *J. Power Sources*, **124**, 432 (2003).

Darwish, N. A., Hilal, N., Versteeg, G. and Heesink, B., "Feasibility of the Direct Generation of Hydrogen for Fuel-Cell-Powered Vehicles by On-board Steam Reforming of Naphtha," *Fuel*, in press (2003).

Lee, D. K., Baek, I. H. and Yoon, W. L., "Modeling and Simulation for the Methane Steam Reforming Enhanced by *in situ* CO_2 Removal Utilizing CaO Carbonation for H_2 Production," *Chem. Eng. Sci*., **59**, 931 (2004).

Ding, Y. and Alpay, E., "Adsoprtion-Enhanced Steam-Methane Reforming," *Chem. Eng. Sci*., **55**, 3929 (2000a).

Ding, Y. and Alpay, E., "Equilibria and Kinetics of CO_2 Adsoprtion on Hydrotalcite Adsorbent," *Chem. Eng. Sci*., **55**, 3461 (2000b).

Elnashaie, S. S. E. H., Adris, A., Al-Ubaid, A. S. and Soliman, M. A., "On the Non-monotonic Behavior of Methane-Steam Reforming Kinetics," *Chem. Eng. Sci*., **45**, 491 (1990).

Ergun, S., "Fluid Flow Through Packed Columns," *Chem. Eng. Prog*., **48**, 89 (1952).

Froment, G. F. and Bischoff, K. B., "Chemical Reactor Analysis and Design," Wiley Publishers, New York (1990).

Han, C. and Harrison, D. P., "Simultaneous Shift Reaction and Carbon Dioxide Separation for the Direct Production of Hydrogen," *Chem. Eng. Sci*., **49**, 5875 (1994).

Hwang, S., "Inorganic Membranes and Membrane Reactors," *Korean J. Chem. Eng*., **18**, 775 (2001).

Hyman, M. H., "Simulate Methane Reformer Reactions," *Hydrocarbon Processing*, **47**, 131 (1968).

Karger, J. and Ruthven, D. M., "Diffusion in Zeolites and Other Microporous Solids," Wiley Publishers, New York (1992).

Knacke, O., Kubaschewski, O. and Hesselmann, K., "Thermochemical Properties of Inorganic Substances I, 2nd Ed.," Springer-Verlag, New York (1991).

Lim, S. Y., Park, B., Hung, F., Sahimi, M. and Tsotsis, T. T., "Design Issues of Pervaporation Membrane Reactors for Esterification," *Chem. Eng. Sci*., **57**, 4933 (2002).

Liu, Z., Roh, H. and Park, S., "Hydrogen Production for Fuel Cells Through Methane Reforming at Low Temperatures," *J. Power Sources*, **111**, 283 (2002).

Nam, S. W., Yoon, S. P., Ha, H. Y., Hong, S. and Maganyuk, A. P., "Methane Steam Reforming in a Pd-Ru Membrane Reactor," *Korean J. Chem. Eng*., **17**, 288 (2000).

Park, B., Ravi-Kumar, V. S. and Tsotsis, T. T., "Models and Simulation of Liquid-Phase Membrane Reactors," *Ind. Eng. Chem. Res*., **37**, 1276 (1998).

Park, B. and Tsotsis, T. T., "Models and Experiments with Pervaporation Membrane Reactors Integrated with an Adsorbent System," *Chem. Eng. and Proc*., **43**, 1171 (2004).

Prasad, P. and Elnashaie, S. S. E. H., "Novel Circulating Fluidized-Bed Membrane Reformer Using Carbon Dioxide Sequestration," *Ind. Eng. Chem. Res*., **43**, 494 (2004).

Sanchez, J. and Tsotsis, T. T., "Catalytic Membranes and Membrane Reactors," Wiley-VCH, Weinheim (2002).

Saracco, G. and Specchia, V., "Catalytic Inorganic-Membrane Reactors: Present Experience and Future Opportunities," *Catal. Rev.-Sci. Eng*., **36**, 305 (1994).

Semelsberger, T. A., Brown, L. F., Borup, R. L. and Inbody, M. A., "Equilibrium Products from Autothermal Processes for Generating Hydrogen-rich Fuel-cell Feeds," *Int. J. Hydrogrn Energy*, in press (2003).

Xiu, G., Li, P. and Rodrigues, A. E., "Sorption-Enhanced Reaction Process with Reactive Regeneration," *Chem. Eng. Sci*., **57**, 3893 (2002).

Xiu, G., Li, P. and Rodrigues, A. E., "Adsorption-Enhanced Steam-Methane Reforming with Intraparticle-Diffusion Limitations," *Chem. Eng. J*., **95**, 83 (2003).

Xu, J. and Froment, G. F., "Methane Steam Reforming, Methanation and Water-gas Shift: I. Intrinsic Kinetics," *AIChE J*., **35**, 88 (1989).